Limit Cycle Estimation and Suppression in Automatic Load Frequency Control of Single and Two-Area Power Systems Using Advanced Control Strategies

KARTIK CHANDRA PATRA*[,a], ASUTOSH PATNAIK
Department of Electrical Engineering
C.V. Raman Global University, Bhubaneswar, Odisha 752054,
INDIA

[a]ORCID ID: 0000-0002-4693-4883

Corresponding Author

Abstract: - To maintain system stability, especially in interconnected grids, a dedicated control strategy is required. This leads to the concept of Load Frequency Control (LFC). There is an ample choice of controllers used in LFC. While PI/PID controllers are popularly used, modern systems increasingly rely on proficient approaches like LQR and Fuzzy Logic Controllers (FLC) for improved control and optimization. We have considered four models of LFC in order to conduct a comparative study based on the primary objective of minimizing the deviation of frequency from its nominal value. Four models are selected. First, a single-area load frequency control system is analyzed through a comparative evaluation of PI, optimal, and fuzzy logic controllers. The second model is selected as an automatic LFC of two area systems using the LQR method, where the controller selects the most advanced optimal solution, which uses the Riccati Equation. The third model is selected, which is expected to render full satisfaction/fulfilment of the basic concept of LFC with the full utilization of battery energy storage system (BESS), wind turbine (WT), photovoltaic (PV), high voltage direct current (HVDC), and synchronous generator (SG). This promise guarantees frequency stability and maintains balanced tie-line power, and proposes a new coordinated frequency control approach for the LFC two area system to enhance frequency stability and address the concerns of low-inertia systems. In the selected models, the primary components are speed governors, turbines, and synchronous generators. The governors have inherent backlash nonlinearity, which is responsible for exhibiting self-sustained oscillations and is otherwise known as Limit Cycles (LC) that needs to be completely mitigated/suppressed for proper functioning of LFC. This has been given necessary weightage, and signal stabilization by Gaussian/ deterministic signal have been adopted after estimation of LC in different models. In order to maintain frequency stability, the challenges of low inertia have been resolved with an LFC hybrid model integrating SG, WT, PV, BESS, and HVDC is proposed in the present work. This promises a guarantee for frequency stability and maintain balanced tie-line power and proposes a new coordinated frequency control strategy for the LFC in two-area systems to maintain the frequency stability and addresses of low inertia.
Our basic objective is to reach the goal of achieving the minimum deviation of frequency in the minimum time with the use of a single controller in the four models selected for their specific performance characteristics, used in a specific environment. We proposed four steps procedure which includes a preliminary test appropriately obtained step response conducted on selected models with governors removing their backlash nonlinearity; secondly the estimation of LC in all models with governors in presence of their backlash nonlinearity, third step elimination of LC by signal stabilization with high frequency deterministic signals/Gaussian (random) signals on the models finally application of digital deadbeat controllers on all models. Besides a simple model included as a sample model which has undergone four steps procedures like other models to achieve guaranteed frequency stability in terms of frequency deviation ($\Delta f=0$, in time $t=0$). The system is modeled and analyzed through simulations carried out in the Simulink environment of MATLAB, yielding the anticipated performance outcomes.

Key-Words: - Estimation and suppression of limit cycles, load frequency control (LFC), Digital Deadbeat Controller (DDC), Area Control Error (ACE), Renewable Energy Sources (RESs), Linear Quadratic Regulator (LQR), Battery Energy Storage System (BESS).

Received: March 6, 2026. Revised: May 9, 2026. Accepted: June 3, 2026. Published: July 6, 2026.

1 Introduction

Within a locality, an isolated power generating units sometimes witness instability due to sudden load variations which consequently, lead to perturbations in the system frequency. Numerous traditional methods were developed to deliver auxiliary control that rapidly re-establish the system frequency at its nominal level. Among these approaches include use of PI [1-3] are employed to regulate the load reference through adjustments to the prescribed speed value. This control objective is called LFC. Supplementary control refers to high renewable penetration and to extra mechanisms added to power grid control, especially with high renewable energy (like wind/solar), to quickly stabilize frequency deviations beyond what standard controls (like governors) offers, using resources like battery storage to manage intermittency and inertia reduction, ensuring grid stability.

The main objective of incorporating integral action is to improve the system type, thereby ensuring zero steady-state frequency deviation, Δf. The resulting control performance is influenced by the governor speed regulation parameter R and the KI (integral gain). Although this approach is straightforward to implement, it often leads to significant transient frequency excursions. To address these shortcomings, optimal control strategies employing state feedback have been introduced [4–6]; however, complete knowledge of all system states is not always readily available in practice.

Adaptive neural network techniques [7–8] have been explored to improve transient and dynamic performance; however, their effectiveness is often constrained by the extensive data requirements and long training times. Fuzzy logic–based approaches have also been widely applied in load frequency control of power systems. For instance, Huge et al. [9] proposed a fuzzy controller to reduce frequency deviations, while Induka et al. [10] developed a fuzzy-based LFC scheme aimed at minimizing the ACE and its rate of change. Additionally, [11] presents development and simulation based on FLC for single-area LFC in an isolated power system environment.

In a single or two-area interconnected power systems, any load disturbance in one area is accommodated collectively by all interconnected areas through adjustments in generation, leading to variations in tie-line power flows and a corresponding drop in system frequency [12]. Under normal operating conditions, the frequency is maintained at its nominal value, tie-line power exchanges remain at scheduled levels.

The model presented in [13] is developed based on the following principle. Frequency deviations are sensed using a frequency sensor, while changes in tie-line power are monitored through the LFC mechanism, which reflects variations in the rotor angle δ. The Δf and tie-line power deviation $\Delta P_{\square ie}$, are processed and combined to form a real power control signal, ΔP_v.

The transfer function (TF) of governor is represented as :1/(1+sTg)

The TF of Turbine is modeled by : 1/(1+sTf)

The TF of generator is given by : 1/(1+sTp)

A controller operates by measuring the value of a controlled variable and comparing it with the desired input. It then determines the error or deviation between the actual and desired values and generates an appropriate control signal as an output. This control signal acts on the system to reduce the deviation, ideally bringing it to zero or to the minimum possible level. In the model, a PI controller in conjunction with the optimal controller like linear LQR is used expecting the result sought. In current applications, the increasing penetration of RESs has reduced the overall inertia. As a result of which the frequency stability becomes more volatile and unpredictable. In order to power systems, the increasing penetration of RESs has reduced the overall system inertia. The reduced inertia yields the frequency stability to become more volatile and unpredictable. Contrary to traditional power plants, using power electronic based/converter based RESs results in their decoupling form the power system making them incapable of directly responding to any frequency disturbance to an AC system [14-15]. The rate of change of frequency (RoCoF) is a crucial measure for assessing the inertia of power system, particularly when RESs is high [16]. RoCoF is becoming important in power systems due to potential for a significant change in RoCoF, leading to trigger load shedding controllers and even causing a blackout [17]. RoCoF guides when to trigger LOAD SHEDDING controllers. It is yet to be established to guarantee the frequency stability by the LFC because of the tie-line power interchanges in the required limit in interconnected power systems [18, 19].

The ACE is typically computed by combining the Δf with the $\Delta P_{\square ie}$. Specifically, it is obtained by multiplying the Δf by the area frequency bias factor and then adding the net $\Delta P_{\square ie}$.. This ACE signal serves as the primary input to the LFC, whose objective is to minimize both the ACE and the deviations in system frequency.

To ensure frequency stability and maintain scheduled tie-line power exchanges, recent studies have proposed advanced coordinated control strategies for multi-area systems. For instance, a novel approach for a two-area LFC system integrates modern energy resources such as battery BESS, WT, HVDC links, and conventional SG. Commonly used methods include PI/PID controllers [21-24], and advanced configurations such as PD–PID cascade controllers [27].

The fuzzy approach has also been introduced to counter face the challenges [28, 29]. Another method of use is optimal controls [30, 31]. In [32], and [33] a robust control has been used to address certain uncertainties. However, there is a growing level of interconnections between asynchronous areas and a considerable distance between generation and load centres. HVDC technology emerges as a high suitable solution to address these challenges. In [30], [34], [35], [36] and [37], the authors have proposed an integrated hybrid HVAC–HVDC system in the LFC model. The simplified models for HVDC links are presented in [34], [35] and [36], but could not support analytical procedures and failed to consider rated capacity, voltage level, converter impedance and HVDC loading. In [38], a virtual inertia approach using derivative control for the LFC model, which integrates the HVDC system with the BESS model. The integration of WT on the LFC is investigated in [28], [30], [33], [39], [40], [41], [42] and [43]. Consequently, an LFC hybrid model integrating SG, WT, PV, BESS and HVDC was proposed in [30], [33], [41], [42] and [43]. These models are applied to represent a high penetration of RES integrated into power systems presently. In briefing the three models selected appropriately for our studies: the first is a simple model [11] which uses PI and fuzzy controllers. The second model [13] emphasizes the most advanced optimal LQR controller uses the Riccati Equation i.e. similar as in [13]. This keeps the frequency at nearly nominal value. The third model [20] presents LFC integrating BESS, WT, HVDC and SG, and guarantees frequency stability and maintains balanced tie-line power. This offers a new coordinated frequency control approach for the LFC in two-area system. These three models have been selected for our study and proposed to apply the digital deadbeat controller, where we expect the guaranteed frequency stability which is yet to be achieved in any other control.

Following this section, the next section 2 gives the step response analysis of the selected system models, including the proposed model. Section 3 aims at the estimation of load changes for all models in the presence of backlash nonlinearity in the governing mechanisms. Section 4 examines the stabilization of system signals under both deterministic and stochastic (Gaussian) disturbances. Section 5 details the design and implementation of the proposed DDC. Finally, Section 6 concludes the paper by recapping the main contributions, highlighting the originality and practical value of the presented method, and suggesting possible avenues for future work.

2 Development and Selection of LFC Models for Interconnected Power Systems

An accurate and realistic mathematical representation is fundamental for the analysis and development of LFC in interconnected power systems. Such a model effectively gives the dynamic behavior and interactions amongst key components, including the turbine, generator, and governor. The continuous load fluctuations and inherent nonlinearities further emphasize the need for an appropriate and reliable modeling approach.

In this section, the step response characteristics of the models presented in [11], [13], and [20] are examined and compared with the proposed model, which incorporates the complete dynamics of the turbine, generator, and governor systems. Figure 1 shows the relationship between Δf and the corresponding variation in load demand. This accounts for variations in the mechanical power outputs of multiple generators, represented as $\Delta P_{\square 1}$, $\Delta P_{\square 2}$, …, $\Delta P_{\square\square}$, to evaluate the collective response of the system under frequency disturbances.

Equation 1 states the steady-state frequency deviation Δf due to a load disturbance for a system with n generators and an equivalent damping coefficient D, [7]:

$$\Delta f = \frac{-P_{Lo}}{\left(\frac{1}{R_1}+\frac{1}{R_2}+\frac{1}{R_3}+\cdots+\frac{1}{R_1}\right)+D}$$

$$= \frac{-P_L}{{}^1/_{R_{eq}}+D} \quad \ldots\ldots\ldots\ldots. (1)$$

where, $R_{eq} = \frac{1}{{}^1/_{R_1}+{}^1/_{R_2}+\cdots+{}^1/_{R_n}}$

The factor R, is given by

$$R\% = \frac{\%\, change\ in\ speed\ (or\ frequency)}{\%\, change\ in\ power\ output} \times 100$$

$$= \frac{\omega_{NLo}-\omega_{FLo}}{\omega_0} \times 100 \ldots\ldots\ldots\ldots. (2)$$

Where, ω_{NLo} and ω_{FLo} denotes the steady state speed with absence of load and full load respectively, and ω_0 corresponds to the nominal value.

Figure 2 illustrates the relationship between the Δf (Hz) and output power (in MW).

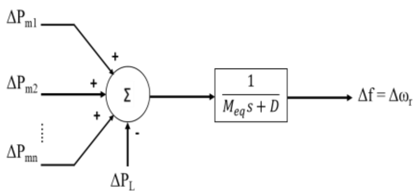

Fig. 1 Equivalent System Model for LFC [7].

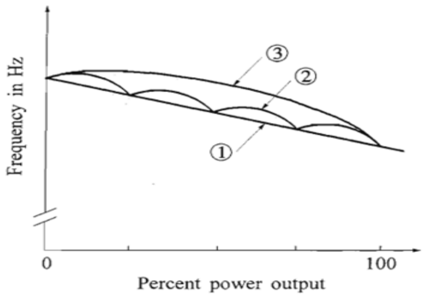

Curve 1: Ideal linear characteristics
Curve 2: Actual characteristics for steam units
Curve 3: Actual characteristics for hydraulic units

Fig. 2 Correlation Between Δf (Hz) and output power (in MW) [7].

2.1 Step Response Analysis of Model [11]

Figure 3(a) illustrates the control system schematic of the model presented in [11]. It represents a single-area power system composed of cascaded turbine, governor, and generator units. The load frequency control is implemented using a PID-based strategy as proposed in [11] to regulate the system.

Figure 3(b) depicts the equivalent step response analysis of the system under a rapid load disturbance (ΔP□). Following the disturbance, the Δf initially exhibits transient behavior but gradually diminishes over time. The system ultimately reaches a steady-state (Δf = 0) after approximately 200 seconds.

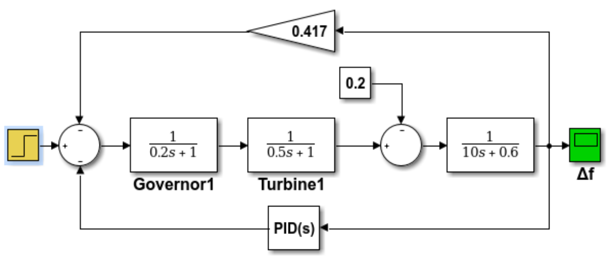

Fig. 3(a) Block diagram of a governor–turbine control system incorporating a PID controller, illustrating the regulation of frequency deviation (Δf) through feedback of the speed signal [11]

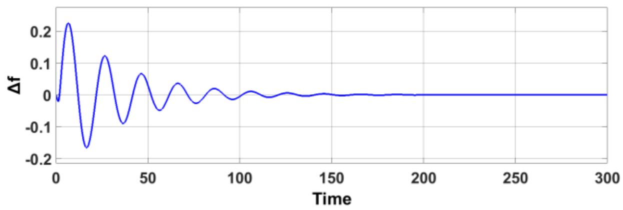

Fig. 3(b) Time response of Δf showing damped oscillations and steady-state stabilization.

2.2 Step Response Analysis of Model [13]

Figure 4(a) illustrates the control system schematic of the model described in [13]. Figure 4(b) shows the equivalent step response analysis of the system when undergoing with load. Following the disturbance, the Δf exhibits a transient response but decreases progressively over time. The system attains steady-state operation (Δf = 0) within approximately 15 seconds.

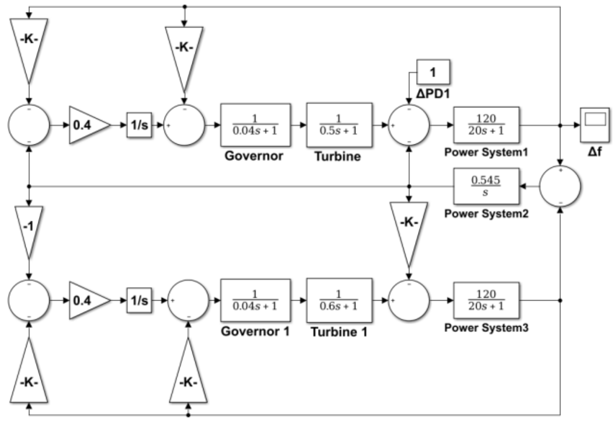

Fig. 4(a) Schematic representation of a multi-area LFC system with interconnected governors, turbines, and tie-line power dynamics [13].

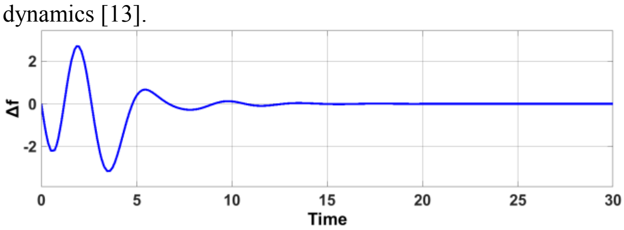

Fig. 4(b) Time response of Δf showing damped oscillations and steady-state stabilization at 15 seconds.

2.3 Step Response Analysis of Model [20]

Figure 5(a) illustrates the control system schematic of the sample model developed in [20]. Figure 5(b) shows the equivalent step response of the system under a sudden load disturbance. Following the disturbance, the Δf gradually decreases over time and eventually reaches the steady-state condition (Δf = 0) after approximately 7500 seconds. This response indicates a significantly slower transient decay compared to other models, highlighting the system's limited dynamic performance in restoring frequency stability.

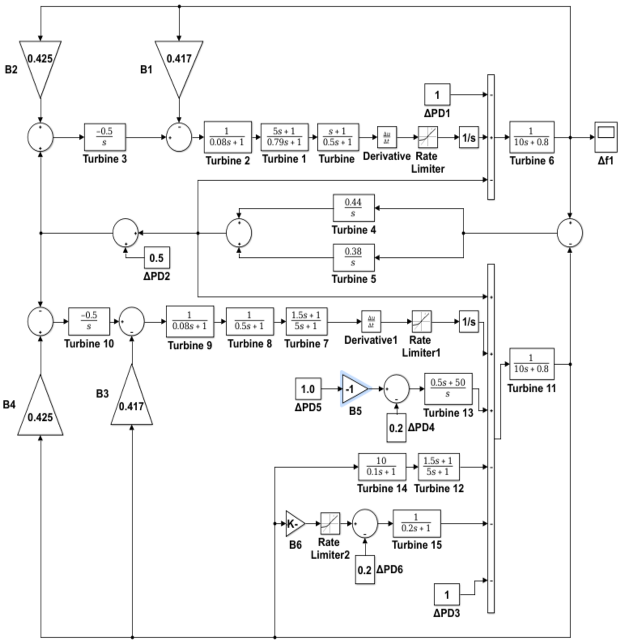

Fig. 5(a) Comprehensive diagram of a two-area LFC system incorporating multiple turbines, governors, derivative units, and area control error (ACE) dynamics [20].

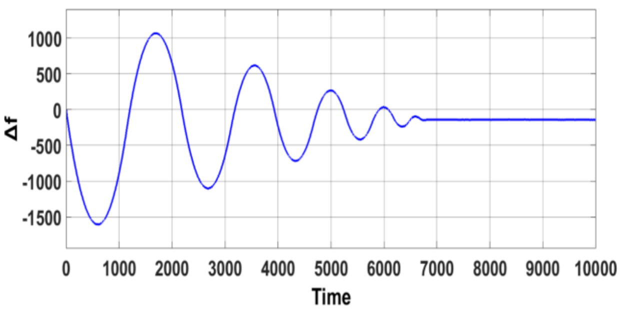

Fig. 5(b) Time response of Δf showing damped oscillations and steady-state stabilization at 7500 seconds.

2.4 LFC model for an interconnected power system based on a modern optimal control approach using a linear quadratic regulator (LQR) [21].

Modern control theory is employed to design an optimal LFC scheme for a SAPS [21]. Accordingly, in the modern control theory approach, single-area optimal LFCs are also developed.

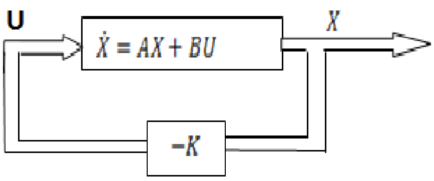

Fig. 6: System with state feedback

In modern control theory, the incremental reference power changes ΔP_{ref1}, and ΔP_{ref2} are treated as control inputs, denoted by u_1 and u_2. In conventional approaches, these control signals are generated by integrating the area control errors (ACEs). However, in modern control practice, u_1 and u_2 are formulated as linear combinations of the system states in a state-feedback configuration or as linear combinations of selected measurable (or controllable) states in an output-feedback configuration.

The quadratic performance is defined as,

$$W = \frac{1}{2}\int_0^\infty (x'Lx + v'Mu)\, dt \;\ldots\ldots (3)$$

Here

L is n × n symmetric positive semi-definite state weighting matrix, x' is the transpose of x, v' is the transpose of v, and M is m × m symmetric positive definite control weighting matrix.

Under autonomous condition the input is $:-K_1x(t)$………. (4)

K_1 is found solving the following equation:

$$P_1A + A'P_1 - \frac{P_1B}{R}B'P_1 + Q = 0 \;\ldots\ldots\ldots\ldots. (5)$$

The optimal state-feedback gain is then computed as:

$$K_1 = \frac{B'P_1}{R} \ldots\ldots\ldots (6)$$

Where A' is the transpose of A, B' is the transpose of B.

An acceptable value of K_1 is one that ensures system stability. Based on Equation (4), the optimal control law can be obtained accordingly, assuming that all system states are measurable and available for feedback implementation. However, measuring and obtaining real-time information for all state variables in large power systems is both difficult and expensive. Under such conditions, an output feedback controller is employed, which is described as follows.

u(t) = -Ky(t)…………. (7)

In case some states are not available, the controllability conditions show the rank of the controllable matrix is not n. In that case, taking into the account the observability conditions, the Riccati equation may be considered for LQG (Linear Quadratic Gaussian) formulation [37]:

$A\Sigma + \Sigma AT + Q0 - \Sigma CT\; R_0^{-1}C\Sigma = 0$ and $L = \Sigma C^T R_0^{-1}$

$\dot{x} = (A - BKC)x(t) = A_C x(t)$………….. (8)

$W = \frac{1}{2}\int_0^\infty (x'L + K'C'KCM)\, x(t)dt$……….. (9)

The control design objective is to determine the optimal gain matrix K that minimizes the performance index W while satisfying the system's state-space dynamics.

$\dot{x} = (A - KBC)x(t)$………….. (10)

Through the application of suitable optimization methods, the corresponding equations for determining the optimal gain matrix are derived.

$0 = A_c^T P + PA_C - C^T K^T MKC + Q$ (11)

$0 = A_c S + S A_c^T + X$ (12)

$K = R^{-1} B^T PSC^T (CSC^T)^{-1}$ (13)

In many practical situations, the initial state vector x(0) is not known, a priori, and such uncertainty is a typical feature of output feedback control design problems. To account for this uncertainty, the design objective is reformulated to minimize the expected value of the performance index, thereby ensuring robust optimal performance in the presence of unknown initial states [22], X = E{J}

$$E\{J\} = \frac{1}{2}E\{x'(0)Px(0)\} = \frac{1}{2}W_0 \ldots\ldots\ldots (14)$$

Where W_0 is the optimal cost is given by transpose of PX.

The value of the feedback, gain, K that minimizes W_0, the three coupled equations must be solved simultaneously. This is typically achieved using suitable iterative numerical techniques [22].

2.4.1 Step response determination for model [21]

Figure 7(a) represents of LFC for single area power system (SAPS) employing LQR controller [21] with a closed-loop control system implemented in Simulink, consisting of cascaded first-order dynamic blocks that model the governor, turbine, and generator dynamics of a power system. The feedback loop incorporates a gain $-K$, which acts as a state-feedback controller to regulate the system output. An integrator block ($1/s$) is included to account for system state accumulation, while the summation junctions combine reference input, feedback signals, and disturbances. Figure 7(b) shows the application of step input response of the model shown in Fig. 7(a) [21]. The system initially exhibits oscillatory behavior with a noticeable overshoot, followed by progressively damped oscillations. The response gradually converges to zero, indicating effective frequency regulation, and a steady-state condition is achieved approximately at 15 seconds.

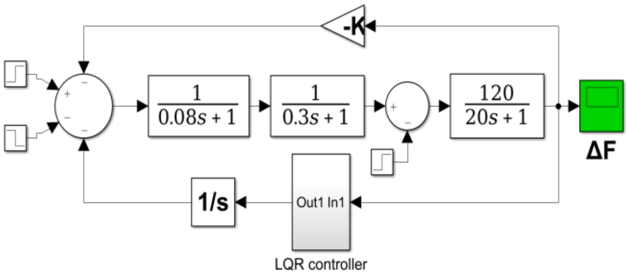

Fig. 7(a) Schematic representation of LFC SAPS employing LQR controller [21]

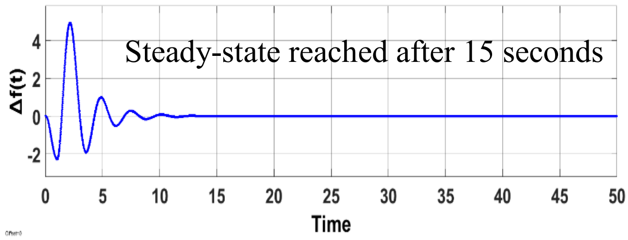

Fig. 7(b) Result showing the response with the application of step input of the model shown in Fig. 4(a) [21]

2.5 Step response determination for Model: (proposed)

Figure 8(a) presents the control system schematic of the proposed model. Figure 8(b) shows the equivalent step response under a sudden load disturbance (ΔP□). Following the disturbance, Δf reaches the steady-state condition in approximately 80 seconds. This result indicates a significantly faster settling time and enhanced dynamic stability when related to the models reported in [11], [13], and [20].

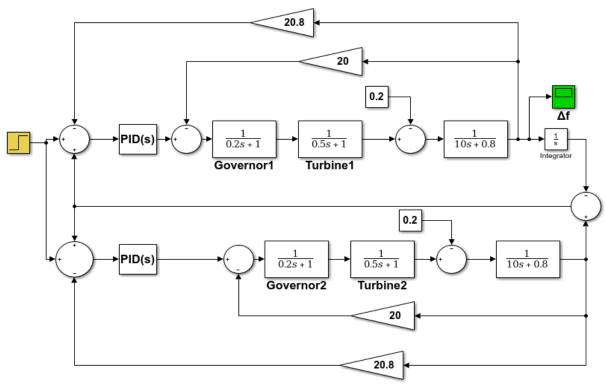

Fig. 8(a) Schematic representation of multi area LFC employing PID controller

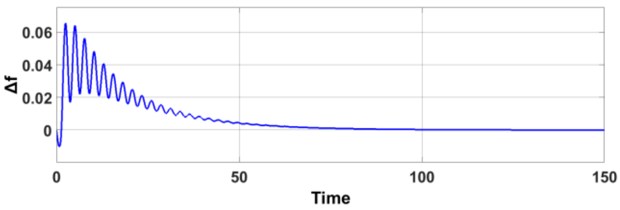

Fig. 8(b) Time response of Δf showing damped oscillations and steady-state stabilization at 80 seconds

3 Estimation of LC

3.1 LC estimation of the model [11]

Figure 9(a) presents the control system schematic of the model proposed in [11]. Figure 9(b) shows the equivalent simulation results, highlighting the occurrence of LC. The system output Δf undergoes persistent oscillations at a frequency near 0.23 rad/s.

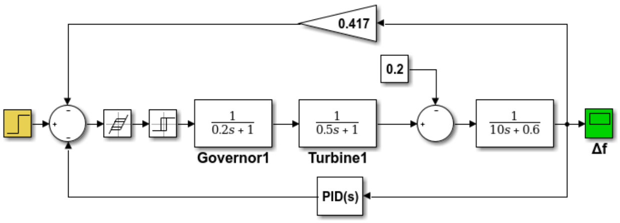

Fig. 9(a) Schematic representation of LFC employing PID controller [11]

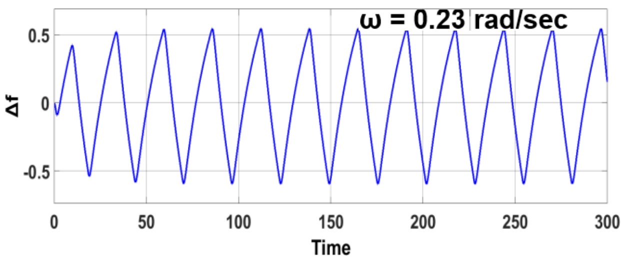

Fig. 9(b) Shows the exhibition of LC.

3.2 LC estimation of the model [13]

The control system schematic representation of the model proposed of [13] is presented in Figure 10(a). Figure 10(b) depicts the corresponding simulation outcomes, which reveal the occurrence of LC behavior in the system response. The Δf shows self-sustained oscillations at an approximate frequency of 1.44 rad/s.

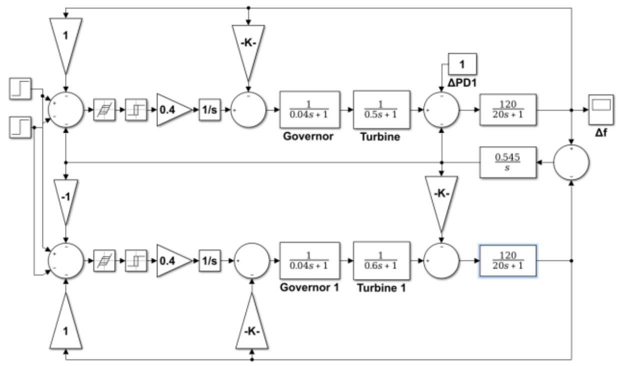

Fig. 10(a) Schematic representation of multi area LFC employing PID controller [13].

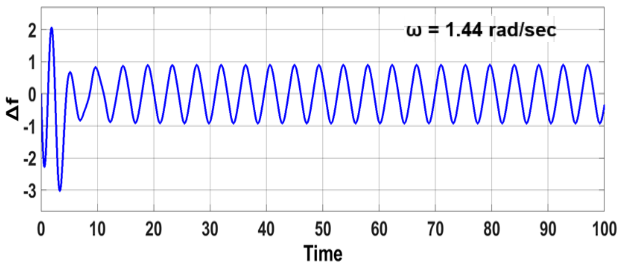

Fig. 10(b) Shows the exhibition of LC whose frequency is 1.44 rad/sec.

3.3 LC estimation of the model [20]

Figure 11(a) presents the control system schematic of the model proposed in [20]. Figure 11(b) shows the equivalent simulation results. The sustained oscillations with a frequency of approximately 0.43 rad/s.

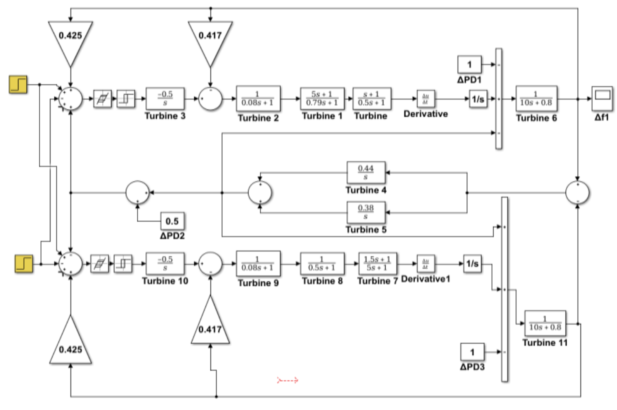

Fig. 11(a) Schematic representation of multi area LFC employing PID controller with BESS [20].

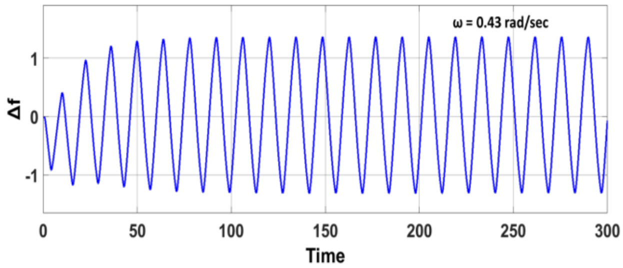

Fig. 11(b) shows the exhibition of LC whose frequency is 0.43 rad/sec.

3.4 Estimation of LC in a single-area power system (SAPS) considering backlash nonlinearity in the speed governor using an optimal Linear Quadratic Regulator (LQR) controller [21].

Figure 12(a) illustrates the complete control system schematic of a SAPS incorporating backlash nonlinearity in the control loop. The governor–turbine–generator dynamics are modeled along with the frequency deviation feedback path. The presence of backlash introduces a dead-band type nonlinearity, which leads to sustained LC in the system response. To mitigate this effect, an LQR controller is integrated into the loop, where optimal state feedback gains are designed based on a quadratic performance index. The diagram clearly shows the interconnection of system components, the location of the backlash element, and the control input path, highlighting how the LQR strategy stabilizes the system and eliminates limit cycles.

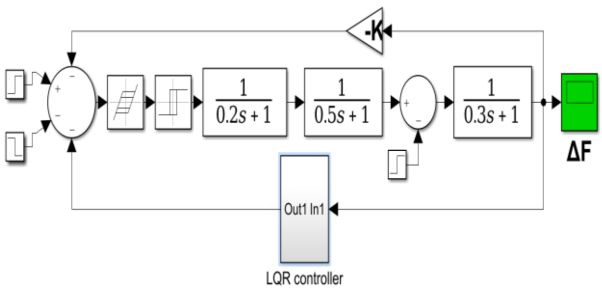

Fig. 12(a): Schematic representation for suppression of LC in SAPS with LQR controller [21]

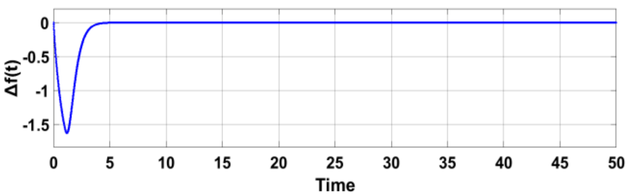

Fig. 12(b) Frequency deviation in SAPS for LFC with LQR controller [21]: The LC is eliminated by the LQR controller.

It is observed in Fig. 12(b) that the LC is completely eliminated due to the presence of the optimal controller, but to reach steady-state, the response takes 15 seconds. Since LC is completely suppressed, the signal stabilization by deterministic signal need not be applied. However, to reduce the settling time signal *stabilization by Gaussian signal to be investigated further for this model* [21].

3.5 LC estimation in the Model (proposed)

Figure 13(a) illustrates the control system schematic of the proposed sample model. Figure 13(b) shows the equivalent output where Δf exhibits sustained self-oscillations with a frequency of approximately 2.24 rad/s.

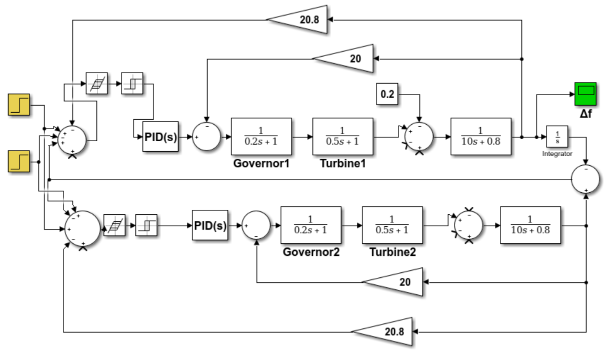

Fig. 13(a) Block diagram of a two-area load frequency control (LFC) system with interconnected governor–turbine units and PID controllers, illustrating the regulation of frequency deviation and tie-line power through feedback control.

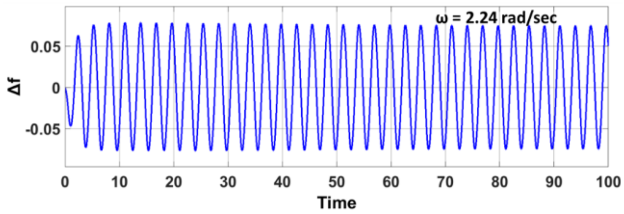

Fig. 13(b) Time-domain response of frequency deviation (Δf), showing sustained oscillations at an angular frequency of approximately 2.24 rad/s.

4 Signal Stabilization

A substantial body of literature has investigated nonlinear characteristics in dynamic systems, including both memoryless nonlinearities (explicit and implicit types) and memory-based nonlinearities such as rectangular hysteresis and backlash effects. It has been widely reported that higher-order linear systems (third order and above), when combined with such nonlinear elements, can exhibit LC oscillations under autonomous operating conditions [44]–[50]. It is emphasized in [55] that the elimination or avoidance of sustained oscillations is essential for the effective implementation of LFC.

The systems examined in Section 3 also exhibit sustained oscillatory behavior, primarily caused by the presence of backlash nonlinearity in the governor mechanism. These oscillations can be mitigated or entirely suppressed by introducing high-frequency dither signals. In practice, the frequency of the dither input is typically chosen to be at least an order of magnitude higher than the limit cycle frequency observed in each model. Such dither signals—whether deterministic or stochastic in nature (e.g., Gaussian noise)—are effective in removing or substantially attenuating these undesirable oscillations while preserving the overall dynamic performance of the system [44], [46], [51], [52].

4.1 Signal Stabilization

4.1.1 Signal Stabilization of Model [11]

Figure 14(a) illustrates the control system schematic of the model proposed in [11]. Figure 14(b) shows that, under this deterministic excitation, the system becomes synchronized with the applied signal, leading to attenuation of oscillatory behavior. Figure 14(c) illustrates the schematic representation of the same model after stabilization using a random Gaussian signal with a mean value of 300 and a variance of 0.25. The stochastic characteristics of this input introduce minor random fluctuations that suppress the periodic oscillations associated with LC behavior. Figure 14(d) demonstrates the successful quenching of LCs and the restoration of stable system operation in the LFC model [11], with the Δf converging to zero.

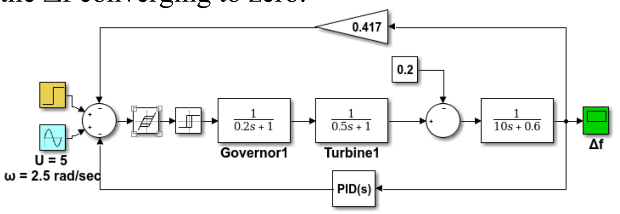

Fig. 14(a) Block diagram of a closed-loop speed control system featuring a governor, turbine dynamics, and PID feedback regulating frequency deviation (Δf).

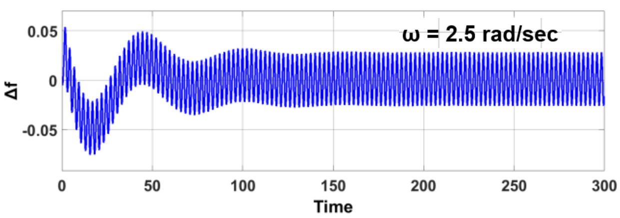

Fig. 14(b) Time response of frequency deviation (Δf) showing an initial oscillatory transient followed by gradual damping and stabilization over time.

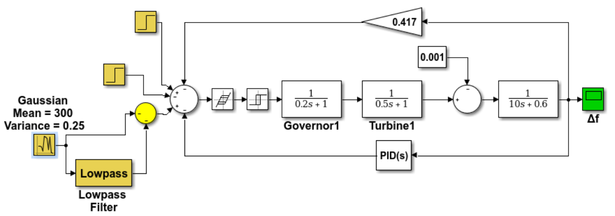

Fig. 14(c) Block diagram of the closed-loop frequency control system with Gaussian noise input passed through a low-pass filter, alongside governor, turbine, and PID controller regulating the frequency deviation (Δf).

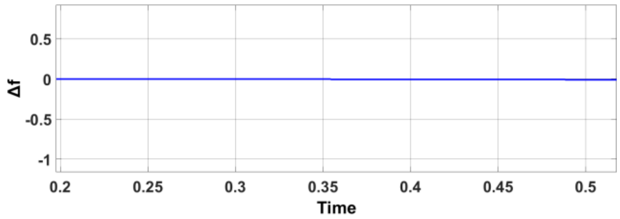

Fig. 14(d) Shows the system is stable and Δf = 0 at steady state (t=0) to the Gaussian signal

4.1.2 Signal Stabilization of Model [13]

Figure 15(a) illustrates the control system schematic of the model proposed in [13]. Figure 15(b) shows that, under the application of this deterministic signal, the system synchronizes with the external excitation, resulting in the attenuation of oscillatory behavior. Figure 15(c) shows the same model after stabilization using a random Gaussian signal with a mean value of 300 and a variance of 0.05. The inherent randomness of this input introduces slight stochastic disturbances that suppress the repetitive oscillations linked to LCs. Figure 15(d) demonstrates the successful suppression of limit cycles and the restoration of stable system operation in the LFC model [13], with the Δf converging to zero.

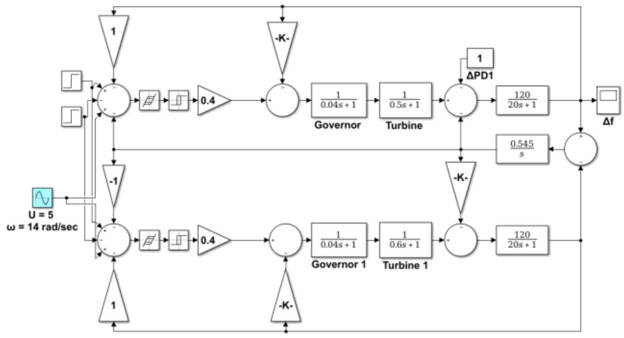

Fig. 15(a) Simulink block diagram of a two-area load frequency control (LFC) system incorporating governor and turbine dynamics, tie-line power exchange, and feedback loops for frequency deviation regulation.

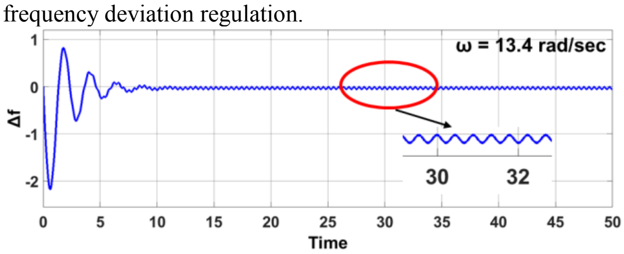

Fig. 15(b) Time-domain response of frequency deviation (Δf) showing transient oscillations and convergence to steady state; inset highlights sustained limit cycle behavior with angular frequency ω = 13.4 rad/s.

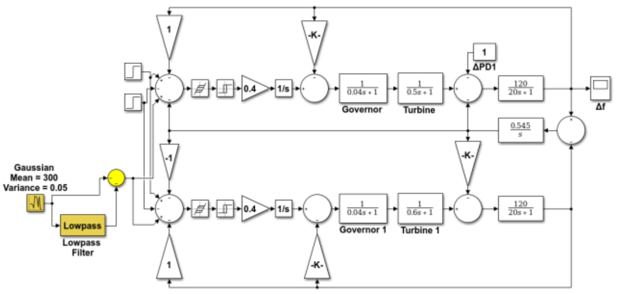

Fig. 15(c) Block diagram of the closed-loop frequency control system (two-area) with Gaussian noise input passed through a low-pass filter, alongside governor, turbine, and PID controller regulating the frequency deviation (Δf) [13]

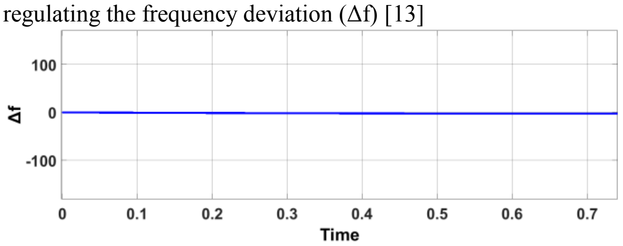

Fig. 15(d) Shows the system is stable and Δf = 0 at steady state (t=0) to the Gaussian signal

4.1.3 Signal Stabilization of Model [20]

Figure 16(a) illustrates the control system schematic of the model proposed in [20]. Figure 16(b) shows that, under this deterministic excitation, the system synchronizes with the applied signal, leading to attenuation of oscillatory behavior. Figure 16(c) depicts the same model under stabilization using a random Gaussian signal with a mean value of 300 and a variance of 0.025. The inherent stochasticity of this input introduces minor perturbations that effectively suppress the periodic oscillations associated with LC behavior. Figure 16(d) demonstrates the successful quenching of LCs and the restoration of stable operation in the LFC model [20], with the Δf converging to zero.

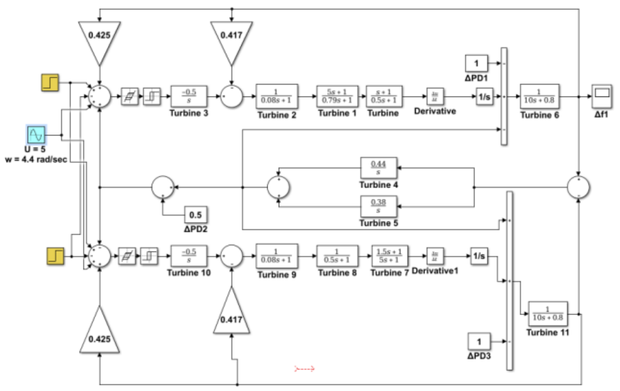

Fig. 16(a) Schematic representation of signal stabilization the model [20] using deterministic signal of 5 sin ωt, where ω = 1 rad/sec

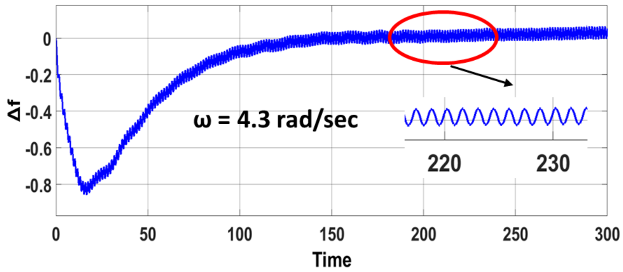

Fig. 16(b) Shows the system are synchronized to the deterministic signal of Fig. 13(a)

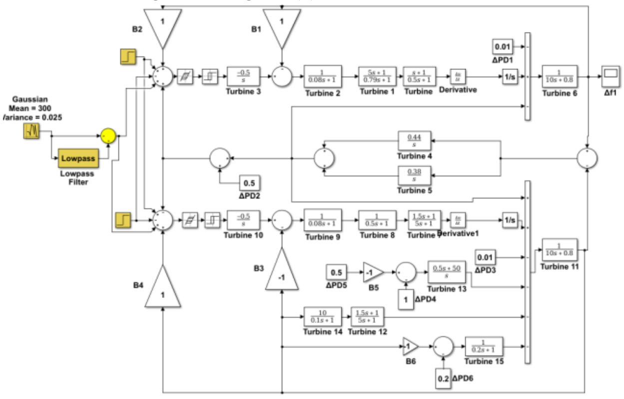

Fig. 16(c) Schematic representation for signal stabilization of the proposed sample model using Gaussian signal of mean – 300 and variance 0.025 [20]

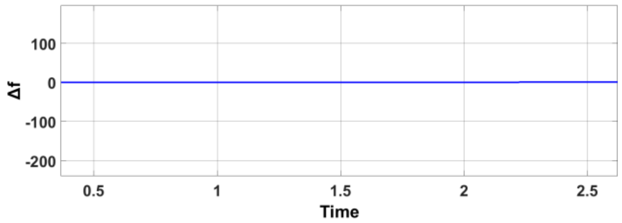

Fig. 16(d) Shows the system is stable and Δf = 0 at steady state (t=0) to the Gaussian signal

4.1.4 Signal Stabilization of Model [21]

Figure 17(a) is a control system schematic showing a Gaussian signal (mean 300, variance 0.05) passed through a low-pass filter (LPF) and supplied to a feedback control loop. It includes a controller and dynamic blocks (transfer functions), which regulate the output ΔF by minimizing disturbances and filtering noise.

Figure 17(b) is a graph showing how Δf varies over time. The curve starts near zero at time zero, drops rapidly into negative values in the first ~40 sec., and then gradually levels off, approaching a steady value around −110. The annotation indicates that a steady state is reached after about 100 seconds, and there are no oscillations because they are eliminated using signal stabilization with Gaussian signals.

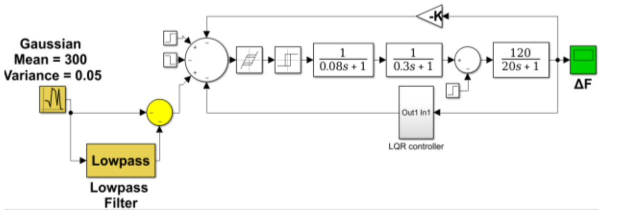

Fig. 17(a) Simulink control system schematic of High-Frequency Gaussian Signal-Based Stabilization for a Single-Area Power System (SAPS) with LQR Controller [21].

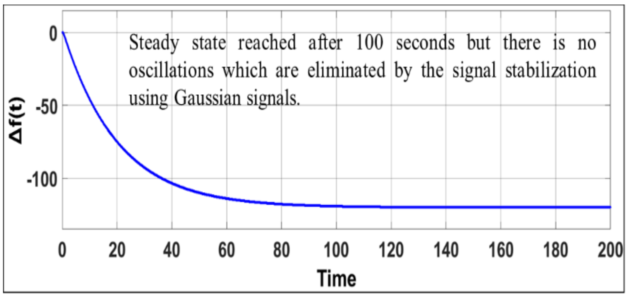

Fig. 17(b) Signal stabilization by high frequency random (Gaussian) signal for SAPS with LQR controller [21]

4.1.5 Signal Stabilization of proposed Model

Figure 18(a) illustrates the control system schematic of the proposed model. Figure 18(b) shows that, under the application of this deterministic signal, the system synchronizes with the external excitation, resulting in the attenuation of oscillatory behavior. Figure 18(c) presents the same model when stabilized using a random Gaussian signal characterized by a mean value of 500 and a variance of 0.25. The stochastic nature of this input introduces small random perturbations that disrupt the periodic oscillations associated with LC behavior. Figure 18(d) demonstrates the successful quenching of limit cycles and restoration of stable operation in the proposed LFC model, with the Δf converging to zero.

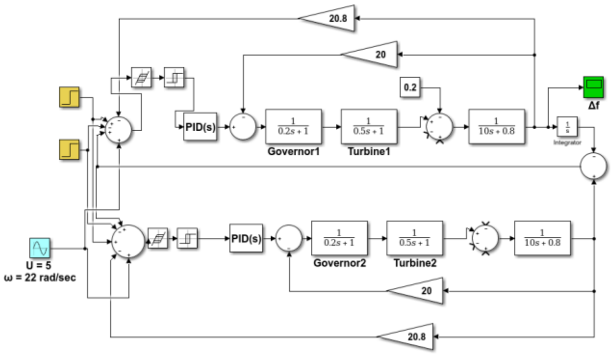

Fig. 18(a) Schematic representation for signal stabilization the sample model using deterministic signal of 5 sin ωt, where ω = 22 rad/sec.

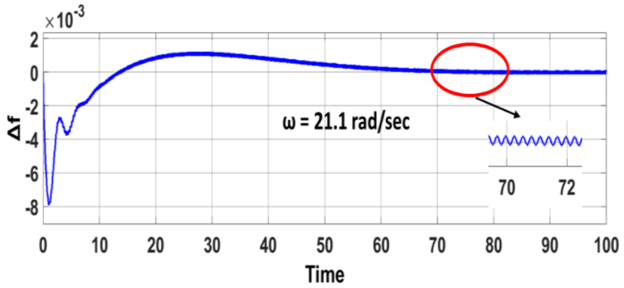

Fig. 18(b) Shows the system are synchronized to the deterministic signal of Fig. 18(a)

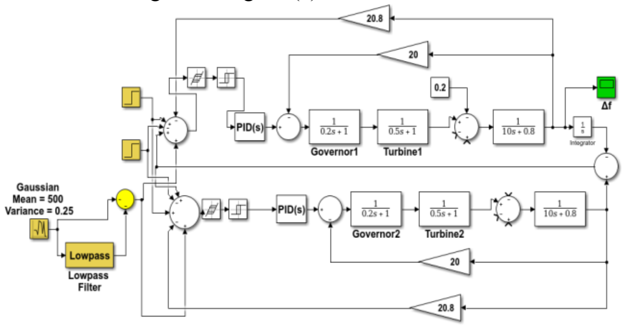

Fig. 18(c) Schematic representation for signal stabilization the proposed sample model using Gaussian signal of mean – 500 and variance 0.025

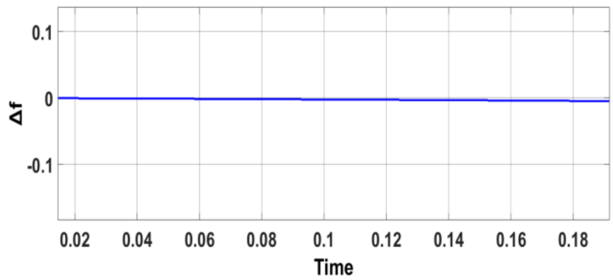

Fig. 18(d) Shows the system is stable and Δf = 0 at steady state (t=0) to the Gaussian signal

5 Comparison of Performances

5.1 Performance Criteria Comparison of Different Controllers

In comparison with other mentioned controllers viz., PI, Optimal and Fuzzy Controller [11], advanced optimal LQR using Riccati equation and using the low inertia RESs [20], the performance of Digital Deadbeat Controller has the following better characteristics.

These results are summarized in Table 1, which compares the LFC performance of different models. The corresponding responses are also illustrated in Fig. 3(b) [11], Fig. 4(b) [13], Fig. 5(b) [20], Fig. 7(b) [21], and for the proposed new model in Fig. 8(b).

5.2 Digital Deadbeat Controller

If the objective is that the output response should reach the desired reference values as quickly as possible and without exhibiting any overshoot. The resulting behavior is generally known as a deadbeat response [53, 54, 56] as shown in Fig. 20(b) [11], Fig. 21(b) [13], Fig. and 22(b) [20].
In order to realize a deadbeat response C(z) must be $1/z^n$ which indicates all the poles must be at origin. Let the z transfer of the cascaded controller shown in Fig. 19(c). For a digital controller system

$$D(z) = \frac{1}{z-1} \times \frac{1}{G_p(z)}$$

where D(z) represents controller transfer function and $G_p(z)$ plant transfer function. Hence D(z) of the open loop system = D(z) * $G_p(z)$ = 1/z-1 * 1/$G_p(z)$ * $G_p(z)$ = 1/z-1. The closed loop system of z transfer function is M(z) = C(z) / R(z) = G(z) /1+ G(z).
For step input: R(z) = Z(1) = z/z-1.
Hence

$$M(z) = \frac{C(z)}{R(z)} = \frac{G(z)}{1+G(z)} = \frac{1/z-1}{1+(1/z-1)} = \frac{1}{z} = \frac{1}{z^1}$$

Hence,

$$C(z) = M(z)R(z) = \frac{1}{z} \times \frac{z}{z-1} = \frac{1}{z-1}$$

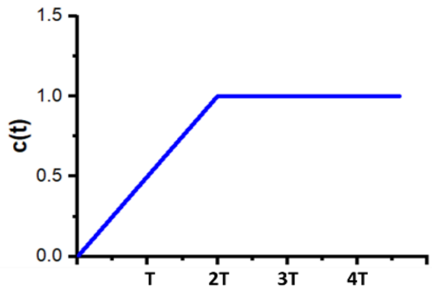

Fig. 19(a) A deadbeat-like response of a continuous-time system to a unit-step input (hypothetical, as an exact deadbeat response is not achievable in continuous-time systems).

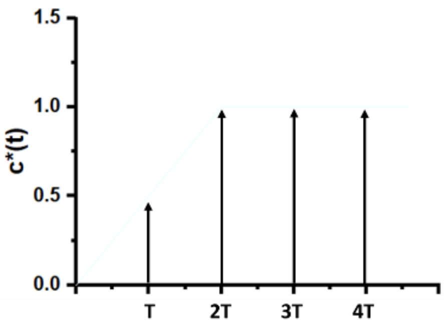

Fig. 19(b) Deadbeat response of a discrete-time system in response to a unit-step input.

For a discrete-time system, achieving a deadbeat response at the sampling instants requires the closed-loop transfer function to be expressed in the following form

$\frac{c(z)}{R(z)} = \frac{1}{Z^n}$ where C(z) $= Z^{-n} + Z^{-n-1} + Z^{-n-2}$+---

"The concept of deadbeat response is inherently associated with discrete-time control systems, and such behavior does not exist in continuous-time control systems [54]. A deadbeat response is achieved when the closed-loop system response to a step input reaches its steady-state value in the minimum possible time, without overshoot, oscillations, or residual ripple between sampling instants. In other words, it represents the fastest possible settling behavior with zero steady-state error and no intermediate fluctuations [54].
Figure 19(c) presents the simplified representation of the DDC-based model, illustrating its basic blocks and the overall control flow within the system.

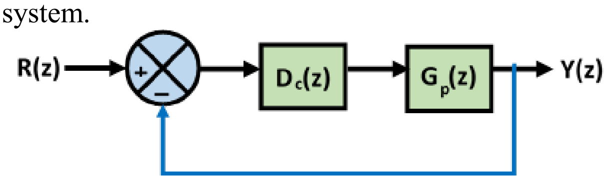

Fig. 19 (c): A simple structure of a Digital Controller

The closed-loop transfer function of the DDC is given by

X(z) = Closed loop transfer function = $\frac{Y(z)}{R(z)} = \frac{1}{Z^n}$ to reach a deadbeat response [52]. During signal stabilization, the input is given at the reference point R(z) (as shown in Figure 15 (c)) that is expressed as U sin ω_ft. The corresponding Z-transform of the input is given by $\frac{U\, z \sin \omega_f T}{z^2 - 2z\cos \omega_f T + 1}$, where n=1.

Hence $\frac{1}{Z^n} = \frac{1}{Z^1} = z^{-1}$

z^{-1} is multiplied with the stabilized or synchronized output signal, as illustrated in Figures 20(a), 21(a), 22(a) and 23(a). The corresponding simulation results and responses are presented in Figures 20(b), 21(b), 22(b) and 23(b), showing the usefulness of the DDC in achieving stable and transient-free performance.

5.3 Application of direct digital control (DDC) in the load frequency control (LFC) model presented in [11].

Figure 20(a) illustrates the control system schematic of the DDC applied to the model presented in [11]. Figure 20(b) shows the corresponding system response, which is characterized by a transient-free and ripple-free behavior, with the frequency deviation converging to zero steady-state error in the minimum possible time. This indicates a near-instantaneous response, signifying the usefulness of the DDC in achieving rapid and precise control.

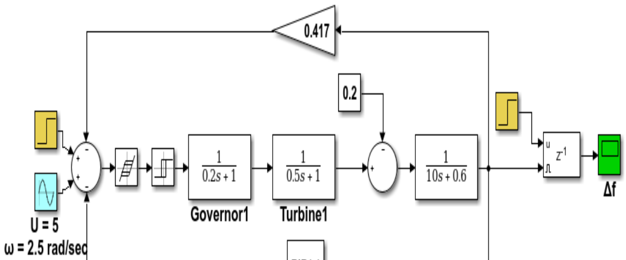

Fig. 20(a) Schematic representation of signal stabilization of the model [11] by DDC

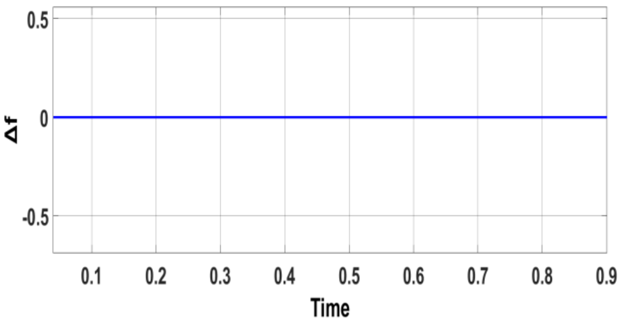

Fig. 20(b) Signal stabilization by DDC of Fig. 20(a)

5.4 Application of DDC in the LFC model presented in [13].

Figure 21(a) illustrates the control system schematic of the DDC applied to the model presented in [13]. Figure 21(b) shows the equivalent system response, which exhibits transient-free and ripple-free behavior, with the frequency deviation converging to zero steady-state error in the minimum possible time. This response demonstrates the high-speed performance of the DDC in achieving rapid and precise regulation within the system.

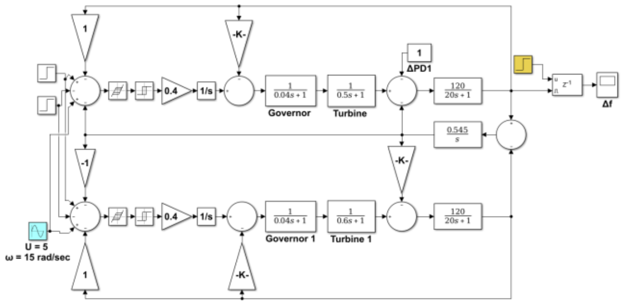

Fig. 21(a) Schematic diagram of signal stabilization for the model in [13] using a digital deadbeat controller implemented in the SIMULINK toolbox with a deterministic input signal.

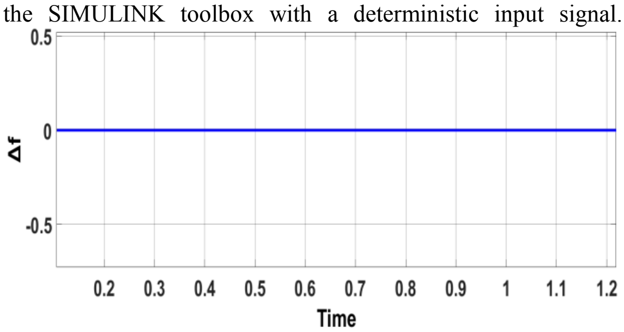

Fig. 21(b) Signal stabilization of Fig. 21(a) using digital deadbeat controller (DDC).

5.5 Application of direct digital control (DDC) in the load frequency control (LFC) model presented in [20].

Figure 22(a) illustrates the control system schematic of the DDC applied to the model presented in [20]. Figure 22(b) shows the equivalent system response, which exhibits transient-free and ripple-free characteristics, with the frequency deviation converging to zero steady-state error in the minimum possible time. This result demonstrates the effectiveness of the DDC in achieving rapid and precise control performance.

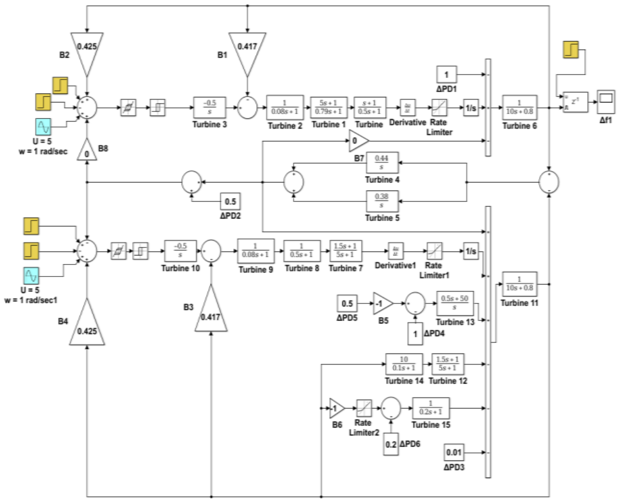

Fig. 22(a) Schematic representation of signal stabilization of the model [20] by digital deadbeat controller using SIMULINK Tool Box with deterministic signal

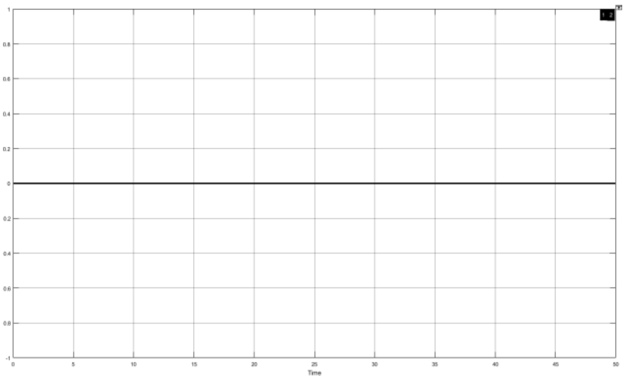

Fig. 22(b) Signal stabilization by digital deadbeat controller of Fig. 22(a)

5.6 Application of DDC in the LFC model presented in [21]

Figure 23(a) illustrates the control system schematic of the DDC applied to the model [21], implemented using the MATLAB environment along with a deterministic stabilizing signal. Figure 23(b) shows the corresponding system response.

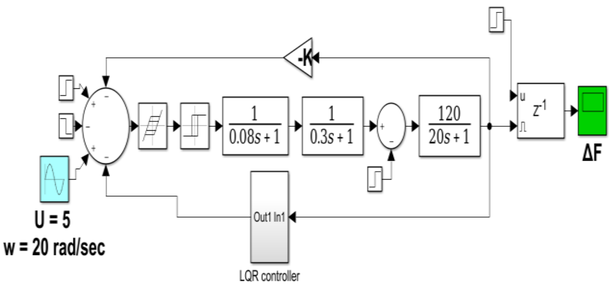

Fig. 23(a) Block diagram representation of SAPS with LFC with deadbeat approach and LQR controller

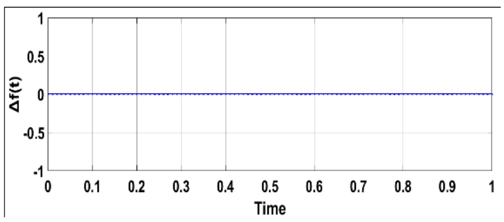

Fig. 23 (b) Frequency deviation in single area LFC with deadbeat approach

5.7 Use of Digital deadbeat controller in the model for LFC (proposed Model)

Figure 24(a) illustrates the control system schematic of the DDC applied to the proposed model, implemented using the MATLAB environment along with a deterministic stabilizing signal. Figure 24(b) shows the corresponding system response, which exhibits transient-free and ripple-free behavior, with the frequency deviation rapidly converging to zero steady-state error in the minimum possible time. This result highlights the superior performance of the proposed control scheme in achieving fast and precise system regulation.

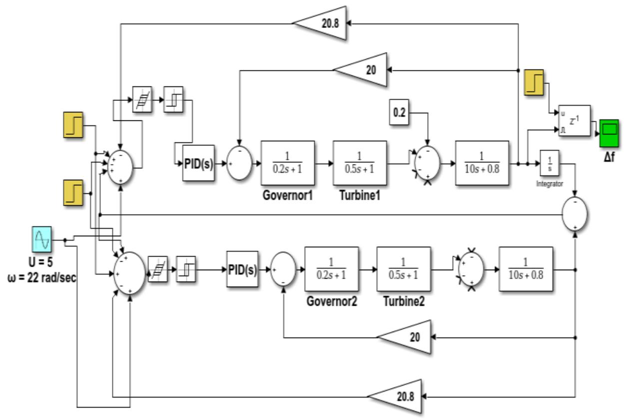

Fig. 24(a) Schematic representation of signal stabilization of the model [20] by digital deadbeat controller using SIMULINK Tool Box with deterministic signal

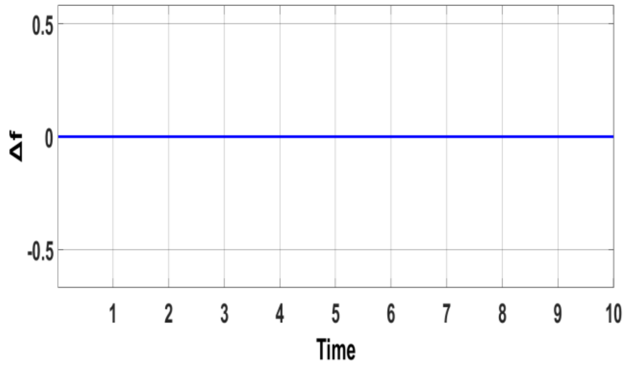

Fig. 24(b) Signal stabilization by digital deadbeat controller of Fig. 24(a)

5.8 Comparison of Results and Discussions

Table 1: Comparison of LFC Performances Using Different Controllers

*ss – steady state

SN	Models	Controllers Used in LFC Applications	Performance in LFC					Remark
			Step Response	Estimation of LC	Signal Stabilization by deterministic Signal	Signal Stabilization by Gaussian Signal	Application of DDC	
1	[11]	PI, Optimal and Fuzzy Controllers	ss Δf=0; transient continuous up to 200 s	LC observed ω=0.23 rad/s	Synchronized to ω=2.5 rad/s	Stabilized fully at ss time taken = 0 seconds Δf equals zero	ss value Δf equals zero Time to reach ss = 0s	Satisfactory (as anticipated)
2	[13]	Advanced Optimal LQR Controller	ss Δf=0; transient continuous up to 15 s	LC observed ω=1.44 rad/s	Synchronized to ω=13.4 rad/s	Stabilized fully at ss time taken = 0 seconds Δf equals zero	ss value Δf equals zero time to reach ss = 0s	Satisfactory (as anticipated)
3	[20]	Uses the Low Inertia RESs	ss Δf=0; transient continuous up to 7500 s	LC observed ω=0.43 rad/s	Synchronized to ω=4.3 rad/s	Stabilized fully at ss time taken = 0 seconds Δf equals zero	ss value Δf equals zero time to reach ss = 0s	Satisfactory (as anticipated)
4	[21]	Optimal LQR & LQG controller	ss Δf=0; transient continuous up to 15 s			Stabilized fully at ss time taken = 100 seconds Δf=0	ss value Δf equals zero time to reach ss = 0s	Satisfactory (as anticipated)
4	**Proposed sample model**	**Digital Deadbeat Controller**	**ss Δf = 0 transient continuous up to 80 s**	**LC observed ω=2.24 rad/s**	**Synchronized to ω=21.1 rad/s**	**Stabilized fully at ss time taken = 0 seconds Δf equals zero**	ss value Δf equals zero **time to reach ss = 0s**	**Satisfactory (as anticipated)**

From the above table, it is observed that signal stabilization by Gaussian (random) the results almost equal to that of DDC. The reason may be stabilizing Gaussian signal uses the frequency component up to the maximum possible value (tends to infinity), which may be due to the low frequency components are filtered by LPF.

6 Conclusion

It is the responsibility of the electricity supply agency/authority to supply the electrical energy/electrical power at nominal frequency (50Hz/60Hz) to every consumer. In the event of sudden demand of load, the generation fails to meet the demand in a reasonable time because of the inertia in main synchronous power generation units which is controlled by the speed governors.

Besides the backlash, nonlinearity present in the governor exhibits LC which deteriorates the performance of the governor. As a result of which grid maintenance is affected due to frequency deviation. It is mandatory to mitigate/totally suppress/quench the LC for appropriate performance of the governor in LFC for stable operation [53]. Further, the problem due to inertia generation can be tackled by the integration of low inertia units such as SG, WT, PV, BESS, and HVDC. The performance of the selected and the proposed sample model have been tested through four steps sequential procedures. The performance of all the models has been concisely presented in Table 1.

It has been observed the proper selection of the controllers in the LFC scheme. The present study has shown the deviation in frequency (Δω=0, in time t=0s). The present findings of realizing zero deviation of frequency within least possible time (t=0) with the digital deadbeat controllers facilitate real time operations and encourages researchers to implement the methodology in real time operation. The specific models [11], [13], and [20] have been selected considering their specific remarkable use of controllers for our study in addition to a simple sample model (proposed).

Acknowledgement

The authors wish to thank the C.V. Raman Global University, Bhubaneswar – 752054, Odisha, India, for providing computer facilities for the preparation of this paper.

References:

[1] Kundur, P., Power System Stability and Control, McGraw – Hill Book Company, New York, 1994.

[2] Saadat, H., Power system Analysis, McGraw – Hill Book Company, New York, 1999.

[3] Aldeen, M. and Marah, J.F., "Decentralized Proportional – Plus-Integral Design Method for Interconnected Power Systems", IEE Proceedings-C, Vol. 138, No. 4, 1991.

[4] Yamashika, K., and Miyagi, H., "Multivariable self-Tuning Regulator for Load Frequency Control System with Interaction of Voltage on Load Demand", IEEE Proceedings-D, Vol. 138, NO. 2, March 1999.

[5] Aldeen M., "A Fresh Approach to the LQR Problems with Application to Power Systems",

Proc. of Int. Power Engineering Conf., Singapore Vol. 1, 1993, Pp. 374 – 379.
[6] Pan, C. I., and Liaw L.M. "AN Adaptive Controller for Power System Load – Frequency Control", IEEE on Power System. Vol. 4, No. 1, Feb. 1989, Pp 122 – 128.
[7] Dyukanovic, M., et.al "Two-Area Load Frequency Control with Neural Networks: Proc. 1993. North American Power Symposium, Pp. 161 – 169.
[8] Brich, A. P, et.al, "Neural Network Assisted Load Frequency Control", 28th University Power Engineering Conf. Proc. Vol. 2, 1993, Pp. 518 – 521.
[9] Hsu, Y., and Cheng, C., "Load Frequency Control using Fuzzy Logic," Int. Conf. on High Technology in the Power Industry, 1991, Pp. 32 – 38.
[10] Indulka, C. S., and Raj, B., "Application of Fuzzy Controller to Automatic Generation Control," Electric Machines and Power Systems, Vol. 23, No. 2, Mar- Apr. 1995, pp. 209 – 220.
[11] Ndubisi S. A single area load frequency control: a comparative study based on pi, optimal and fuzzy logic controllers. American Journal of Scientific and Industrial Research [Internet]. 2011 Oct 1;2(5):748–54
[12] IOSR Journal of Engineering The State Space Modeling of Single, Two and Three ALFC of Power System Using Integral Control and Optimal LQR Control Method (Nilay kumar N. Shah, Chetan D. Kotwal)
[13] Shah, N. N., & Pandit, M. A. R. (2016). Automatic Load Frequency Control of Two Area System Using LQR Method. Int. J. Curr. Eng. Sci. Res., 4(6), 2394-0697.
[14] M. Mehrabankhomartash, M. Saeedifard, and A. Yazdani, ''Adjustable wind farm frequency support through multi-terminal HVDC grids,'' IEEE Trans. Sustain. Energy, vol. 12, no. 2, pp. 1461–1472, Apr. 2021.
[15] D.-T. Trinh, Y.-K. Wu, and M.-H. Pham, ''Adaptive frequency control strategy for PMSG-based wind turbines with improved rotor speed recovery,'' IEEE Access, vol. 12, pp. 63853–63864, 2024.
[16] C.-H. Lin andY.-K.Wu, ''Coordinated frequency control strategy for VSCHVDC-connected wind farm and battery energy storage system,'' IEEE Trans. Ind. Appl., vol. 59, no. 5, pp. 5314–5328, Sep. 2023.
[17] Y.-L. Hu and Y.-K. Wu, ''Inertial response identification algorithm for the development of dynamic equivalent model of DFIG-based wind power plant,'' IEEE Trans. Ind. Appl., vol. 57, no. 3, pp. 2104–2113, May 2021.
[18] Y. Wang, Z. Wang, J. Gan, H. Zhang, and R. Wang, ''Switched observer based adaptive event-triggered load frequency control for networked power systems under aperiodic DoS attacks,'' IEEE Trans. Smart Grid, vol. 14, no. 6, pp. 4816–4826, Nov. 2023.
[19] Y. Wang, Y. Liu, X. Yu, and H. Zhang, ''Jointed observer-based sliding mode predictive control for interconnected power systems with input delays,'' IEEE Trans. Autom. Sci. Eng., early access, Jan. 25, 2024, doi: 10.1109/TASE.2024.3353166.
[20] Trinh DT, Wu YK, Pham MH. A novel load frequency control strategy for a modern power system by considering State-Space modeling and stability analysis. IEEE Access [Internet]. 2024
[21] Parmar, K. S., Majhi, S., & Kothari, D. (2012). Load frequency control of a realistic power system with multi-source power generation. International Journal of Electrical Power & Energy Systems, 42(1), 426–433.
[22] F. Llewis and V. L. Syrmos, Optimal Control, Prentice hall, Englewood cliffs, New Jersy,1995
[23] H. Gozde and M. C. Taplamacioglu, ''Automatic generation control application with craziness based particle swarm optimization in a thermal power system,'' Int. J. Electr. Power Energy Syst., vol. 33, no. 1, pp. 8–16, Jan. 2011.
[24] E. S. Ali and S. M. Abd-Elazim, ''Bacteria foraging optimization algorithm based load frequency controller for interconnected power system,'' Int. J. Electr. Power Energy Syst., vol. 33, no. 3, pp. 633–638, Mar. 2011.
[25] C. K. Shiva, G. Shankar, and V. Mukherjee, ''Automatic generation control of power system using a novel quasi-oppositional harmony search algorithm,'' Int. J. Electr. Power Energy Syst., vol. 73, pp. 787–804, Dec. 2015.
[26] D. Guha, P. K. Roy, and S. Banerjee, ''Load frequency control of large scale power system using quasi-oppositional grey wolf optimization algorithm,'' Eng. Sci. Technol., Int. J., vol. 19, no. 4, pp. 1693–1713, Dec. 2016.
[27] P. Dash, L. C. Saikia, and N. Sinha, ''Automatic generation control of multi area thermal system using bat algorithm optimized PD-PID cascade controller,'' Int. J. Electr. Power Energy Syst., vol. 68, pp. 364–372, Jun. 2015.
[28] H.Wang and Z. S. Li, ''Multi-area load frequency control in power system integrated with wind farms using fuzzy generalized predictive control method,'' IEEE Trans. Rel., vol. 72, no. 2, pp. 737–747, Jun. 2023.
[29] X. Li and D. Ye, ''Event-based distributed fuzzy load frequency control for multiarea nonlinear power systems with switching topology,'' IEEE Trans. Fuzzy Syst., vol. 30, no. 10, pp. 4262–4272, Oct. 2022.
[30] A. Elmelegi, E. A. Mohamed, M. Aly, E. M. Ahmed, A. A. Mohamed, and O. Elbaksawi, ''Optimized tilt fractional order cooperative controllers for preserving frequency stability in renewable energy-based power systems,'' IEEE Access, vol. 9, pp. 8261–8277, 2021.
[31] S. Trip, M. Cucuzzella, C. De Persis, A. van der Schaft, and A. Ferrara, ''Passivity-based design of sliding modes for optimal load frequency

control,'' IEEE Trans. Control Syst. Technol., vol. 27, no. 5, pp. 1893–1906, Sep. 2019.

[32] D. Rerkpreedapong, A. Hasanovic, and A. Feliachi, ''Robust load frequency control using genetic algorithms and linear matrix inequalities,'' IEEE Trans. Power Syst., vol. 18, no. 2, pp. 855–861, May 2003.

[33] N. Vafamand, M. M. Arefi, M. H. Asemani, and T. Dragicevic, ''Decentralized robust disturbance-observer based LFC of interconnected systems,'' IEEE Trans. Ind. Electron., vol. 69, no. 5, pp. 4814–4823, May 2022.

[34] B. K. Sahu, T. K. Pati, J. R. Nayak, S. Panda, and S. K. Kar, ''Anovel hybrid LUS-TLBO optimized fuzzy-PID controller for load frequency control of multi-source power system,'' Int. J. Electr. Power Energy Syst., vol. 74, pp. 58–69, Jan. 2016.

[35] Y. Arya and N. Kumar, ''AGC of a multi-area multi-source hydrothermal power system interconnected via AC/DC parallel links under deregulated environment,'' Int. J. Electr. Power Energy Syst., vol. 75, pp. 127–138, Feb. 2016.

[36] E. Sahin, ''Design of an optimized fractional high order differential feedback controller for load frequency control of a multi-area multi-source power system with nonlinearity,'' IEEE Access, vol. 8, pp. 12327–12342, 2020.

[37] N. Pathak, A. Verma, T. S. Bhatti, and I. Nasiruddin, ''Modeling of HVDC tie links and their utilization in AGC/LFC operations of multiarea power systems,'' IEEE Trans. Ind. Electron., vol. 66, no. 3, pp. 2185–2197, Mar. 2019.

[38] E. Rakhshani and P. Rodriguez, ''Inertia emulation in AC/DC interconnected power systems using derivative technique considering frequency measurement effects,'' IEEE Trans. Power Syst., vol. 32, no. 5, pp. 3338–3351, Sep. 2017.

[39] T. H. Mohamed, J. Morel, H. Bevrani, and T. Hiyama, ''Model predictive based load frequency control design concerning wind turbines,'' Int. J. Electr. Power Energy Syst., vol. 43, no. 1, pp. 859–867, Dec. 2012.

[40] N. Nguyen and J. Mitra, ''An analysis of the effects and dependency of wind power penetration on system frequency regulation,'' IEEE Trans. Sustain. Energy, vol. 7, no. 1, pp. 354–363, Jan. 2016.

[41] G. Magdy, H. Ali, and D. Xu, ''Effective control of smart hybrid power systems: Cooperation of robust LFC and virtual inertia control system,'' CSEE J. Power Energy Syst., vol. 8, no. 6, pp. 1583–1593, Nov. 2021.

[42] J. Cao, W. Du, H. Wang, and M. McCulloch, ''Optimal sizing and control strategies for hybrid storage system as limited by grid frequency deviations,'' IEEE Trans. Power Syst., vol. 33, no. 5, pp. 5486–5495, Sep. 2018.

[43] B.-K. Chiu, K.-Y. Lee, and Y.-Y. Hsu, ''Battery energy storage system damper design for a microgrid with wind generators participating in frequency regulation,'' Energies, vol. 16, no. 21, p. 7439, Nov. 2023.

[44] Patra, K.C., Patnaik, A., Estimation of Limit Cycles and Signal Stabilization with Deadbeat approach in three Dimensional Nonlinear systems. International Journal of Control Systems and Robotics, Volume 10, pp. 22-38, 2025. (IF 1.93) (Pub. Date: 31 July 2025, Bulgaria, Europe)

[45] Patra, K.C., Patnaik, A., Load Frequency Control by Speed Governors of Two-Area Power System using Digital Controller with Deadbeat Approach," International Journal of Electrical Engineering and Computer Science, vol. 7, pp. 200-217, 2025, DOI:10.37394/232027.2025.7.19

[46] Patra, K.C., Patnaik, A., Investigation of Limit Cycles and Signal Stabilization by Deterministic and Gaussian Random Signals Based on Deadbeat Approach in 3×3 Nonlinear Systems with Memory Nonlinearities," International Journal of Electrical Engineering and Computer Science, vol. 7, pp. 159-188, 2025, DOI:10.37394/232027.2025.7.17

[47] Patra, K.C., Kar, N., Suppression limit cycles in 2×2 nonlinear systems with memory type nonlinearities. International Journal of Dynamics and Control, 10, 2022, 721-733.

[48] Oldenburger, R.T. Nakada, T. Signal stabilization of Self Oscillating System, IRE Transactions on Automatic Control, vol. 6, no. 3, 1961, 319-325

[49] Gelb, A. and Vander-Velde, W.E Multiple-input describing functions and nonlinear system design, McGraw- Hill, New York, 1968

[50] Atherton, D.P Non-linear control engineering - Describing function analysis and design. Van Noslrand Reinhold, London, 1975

[51] Sah SV, Prakash V, Pathak PK, Yadav AK. Fractional Order AGC design for power systems via artificial Gorilla Troops Optimizer. IEEE [Internet]. 2022 Dec 14;1–6

[52] Hussain J, Zou R, Wu Z, Pathak PK, Akhtar S. Design and performance analysis of Walrus Optimization Algorithm (WAOA)- Based Cascade Controller for load frequency control of a Multi- Area power system with renewable sources. International Journal of Numerical Modelling Electronic Networks Devices and Fields [Internet]. 2025 Mar 1;38(2)

[53] Benjamin, C., Kuo, Digital Control Systems, Oxford University Press, 2nd Edition, 8th Impression, 2009.

[54] Ogata. K., Discrete-time control systems. Prentice-Hall, Inc., 2nd Edition, 1995.

[55] Tsay TS. Load–frequency control of interconnected power system with governor backlash nonlinearities. International Journal of Electrical Power & Energy Systems [Internet]. 2011 Aug 6;33(9):1542–9.

[56] Raymond T. Stefani, Bahram Shahian, Clement J. Savant, Jr., Gene H. Hostetter, Design of Feedback Control Systems 4th Ed, OXFORD UNIVERSITY PRESS, 2002

Contribution of Individual Authors to the Creation of a Scientific Article (Ghostwriting Policy)

Kartik Chandra Patra has formulated the problem, methodology of analysis adopted and algorithm of computation presented.
Asutosh Patnaik has made the validation of the results using the geometric tools and SIMULINK toolbox of MATLAB software.

Sources of Funding for Research Presented in a Scientific Article or Scientific Article Itself

No funding was received for conducting this study.

Conflict of Interest

The authors have no conflicts of interest to declare that are relevant to the content of this article.